

Strain-Induced Grain Growth during Rapid Thermal Cycling of Aluminum Interconnects

R.R. KELLER, R.H. GEISS, N. BARBOSA III, A.J. SLIFKA, and D.T. READ

We demonstrate the rapid growth of grains in nonpassivated, sputtered Al-1 at. pct Si interconnects during 200 Hz thermal cycling induced by alternating current. Mean grain diameters were observed by use of automated electron backscatter diffraction (EBSD) to increase by more than 70 pct after an accumulated cycling time of less than 6 minutes over a temperature range of 200 °C, which corresponded to a total strain range of 4×10^{-3} . Plasticity in growing grains primarily took the form of topography formation at the free surface and grain rotation, while consumed grains tended to retain relatively high dislocation content. Grain growth was characterized by means of pairwise comparisons in EBSD pattern quality across moving boundaries. Out of 92 cases where a grain was observed to grow into its neighbor, 61 cases indicated that the growing grain had a higher average pattern quality factor than that of the consumed grain, at the 95 pct confidence level. The results are consistent with a strain-induced boundary migration mechanism, wherein stored plastic strain energy differences from grain to grain drive growth, some of which was observed after only 10 seconds of cycling.

DOI: 10.1007/s11661-006-9017-1

© The Minerals, Metals & Materials Society and ASM International 2007

I. INTRODUCTION

WE describe the evolution of microstructure associated with thermal cycling of patterned interconnects induced by low-frequency, high-density alternating currents. Reliability issues associated with thermal fatigue center on failures that take place after accumulation of cyclic strain. Examples include resistivity increases due to the introduction of excessive lattice defects,^[1] brittle film cracking due to deformation of underlying metal films,^[2] or open circuits due to metal deformation.^[3] Thermal fatigue testing and characterization of thin metal films is most often performed by thermally cycling blanket films or arrays of patterned lines in a furnace and observing the stress-strain response through wafer curvature measurements.^[4–7] While useful for blanket films or large arrays of lines, this measurement method is limited in its applicability to an individual patterned line, especially if that line is buried beneath other materials. Fatigue studies of individual patterned structures have been accomplished through methods such as cyclic cantilever beam bending^[8] and microtensile testing.^[9] Such studies have shown that fatigue processes in dimensionally constrained materials can be consider-

ably different from those known to operate in bulk forms of the same materials. For instance, thinner films showed improved fatigue resistance over thicker films, as well as fewer surface extrusions.^[8] However, these methods still cannot adequately address the cyclic behavior of lines of width less than 10 μm or buried structures.

Thermal fatigue testing by means of alternating currents is a relatively unexplored method for inducing cyclic deformation in individual patterned structures, holding potential for testing of individual buried lines. The method is based on controlled joule heating of an interconnect on a substrate, induced by a low-frequency, high-density alternating current, under conditions that preclude electromigration. Details of the test method are provided elsewhere.^[10] For a metal film or line well adhered to a substrate, the magnitude of the mismatch in coefficients of thermal expansion ($\Delta\alpha$), in combination with the temperature change (ΔT) induced by the current in one power cycle, determines the cyclic thermal strain range $\Delta\varepsilon$ through the relation

$$\Delta\varepsilon = \Delta\alpha \cdot \Delta T \quad [1]$$

Because the substrate is massive compared to the film or line, the metal undergoes straining over nearly the entire range expressed in Eq. [1].

Choice of frequency is an important factor. At electrical frequencies much greater than 10 kHz, the efficiency of heat dissipation into the substrate decreases substantially;^[10] we note that strain cycles at the same frequency as the power, which is twice the electrical frequency. The resulting cyclic strain causes several types of characteristic damage within patterned polycrystalline metal lines. For example, severe surface

R.R. KELLER, Group Leader, R.H. GEISS, NIST Affiliate, N. BARBOSA III, Research Engineer, A.J. SLIFKA, Research Engineer, and D.T. READ, Physicist, are with the Materials Reliability Division, National Institute of Standards and Technology, Boulder, CO 80305, USA. Contact e-mail: bob.keller@nist.gov

This article is based on a presentation given in the symposium entitled "Deformation and Fracture from Nano to Macro: A Symposium Honoring W. W. Gerberich's 70th Birthday" which occurred during the TMS Annual Meeting, March 12–16, 2006, in San Antonio, Texas and was sponsored by the Mechanical Behavior of Materials and Nanomechanical Behavior Committees of TMS.

Article published online January 18, 2007.

topography has been observed in selected regions in nonpassivated aluminum^[3] and copper.^[10,11] The damaged regions exhibited periodicity that is consistent with slip processes that took place during cyclic straining. Continued cycling resulted in the spreading of damage to larger volumes of the film.

In both aluminum and copper, grains damaged during rapid thermal cycling were also observed to grow, consuming neighboring grains.^[11,12] However, in the absence of quantitative measurements of the localized characteristics of grain growth induced by this type of cycling, no suggestions as to the mechanism governing grain growth have yet been made. In this work, we present such measurements of grain growth in an Al-1 at. pct Si line subjected to progressively increasing numbers of thermal cycles, in a quasi *in-situ* test incorporating electrically induced cycling coupled with automated electron backscatter diffraction (EBSD) and field emission-scanning electron microscopy (FE-SEM). The observations are discussed in terms of local variations in grain to grain plasticity.

II. EXPERIMENTAL

Electrical tests were carried out on nonpassivated, single-level structures composed of patterned and etched Al-1 at. pct Si lines sputtered onto thermally oxidized silicon. We used a NIST-2 test pattern originally designed for electromigration and thermal conductivity measurements.^[13] The particular line described in this experiment was 800- μm long, 3.3- μm wide, and 0.5- μm thick, with current pads and voltage taps at each end. Testing was conducted in current control on a four-point probe station using 100 Hz sinusoidal alternating currents with zero direct current offset. Current was supplied with a current calibrator, which was driven by an arbitrary waveform generator; current was measured with an uncertainty of 0.06 mA. The line cross section was measured to within 0.05 μm^2 . For this test, a root-mean-square (rms) current density of 12.2 MA/cm² was applied, with an uncertainty of 0.3 MA/cm². The chip was held in place on a stainless steel stage with a vacuum chuck during testing. The stage remained nominally at room temperature; a thermocouple attached to the chip with silver paste indicated a time-averaged temperature rise of approximately 2 °C to 3 °C during cycling. The cyclic temperature range corresponding to this rms current density was approximately 200 °C, corresponding to a total strain range of 0.4 pct per power cycle.

A quasi *in-situ* test was carried out by use of field emission SEM and automated EBSD, alternating with progressively increasing numbers of power cycles. The FE-SEM and EBSD data were collected from the entire line prior to testing, establishing the as-deposited condition. The line was then subjected to testing for 10 seconds and removed from the probe station for another series of EBSD measurements. The line was subjected to another 10 seconds of testing, and so on. In this manner, we collected SEM and EBSD data after the following accumulated times (in seconds): 0, 10, 20, 40,

80, 160, and 320. The specimen eventually failed by open circuit at 697 seconds.

The EBSD measurements were made at an incident beam energy of 15 keV and specimen tilt of 70 deg. Orientation mapping was done only over regions of size 20 $\mu\text{m} \times 3 \mu\text{m}$ in a single scan, repeated over the line length, to minimize effects of specimen drift; the resulting maps were then assembled into composite images. Scan times were typically less than 5 minutes for the collection of each 20 $\mu\text{m} \times 3 \mu\text{m}$ region at a step increment of 200 nm, with 8 \times 8 binning. We defined grains as having a minimum of five contiguous pixels with a total orientation variation of no more than 5 deg total angular spread across all contiguous pixels. The particular values in defining a minimum grain size and maximum angular spread were chosen somewhat arbitrarily, but ensured that the data were not strongly biased by isolated pixel errors or incorrectly indexed patterns due to small-particulate contamination during the scan. Grain boundaries were defined by a minimum of a 3 deg average but discrete misorientation change from one grain to the next. We did not distinguish low-angle from high-angle boundaries in the analyses. All EBSD orientation maps are shown in the as-collected state, with no software-imposed filtering or clean-up algorithms applied.

We analyzed intensively a 100 $\mu\text{m} \times 3 \mu\text{m}$ area on the tested structure for quantitative changes in EBSD pattern quality throughout the course of the test, providing information about grain growth. A total of 92 cases, where one grain began to consume an adjacent grain, were analyzed through six time increments (*i.e.*, through the 320-second increment); a total of 77 cases, where no clear grain growth occurred, were also monitored as a control during the same time increments. The definition of a moving boundary was somewhat arbitrary, but generally involved the shift of several adjacent pixels of a grain boundary by approximately 0.2 μm (the EBSD step size) or more from one time-step to the next.

Longitudinal cross-sectional transmission electron microscope (TEM) specimens were prepared from the line after failure (697 seconds, or 1.39×10^5 cycles) by focused ion beam (FIB) milling. The TEM imaging was performed at an incident beam energy of 200 keV to reveal the defect structures induced by thermal cycling.

III. RESULTS

Figure 1 shows a sequence of SEM/orientation map pairs corresponding to the time-steps of (0, 40, 80, 160, and 320 seconds) of accumulated cycling. Each orientation map is positioned in the figure to correspond to the region displayed in the SEM image above it; note that the EBSD data were readily obtained from virtually the entire line segment, including regions exhibiting severe topography. The colors in the orientation maps represent crystal directions lying parallel to the line direction, as given by the inverse pole figure legend in Figure 2; this color representation more clearly distinguishes individual grains than the more conventionally used surface normal representation. The progression of surface damage is apparent from the SEM images.

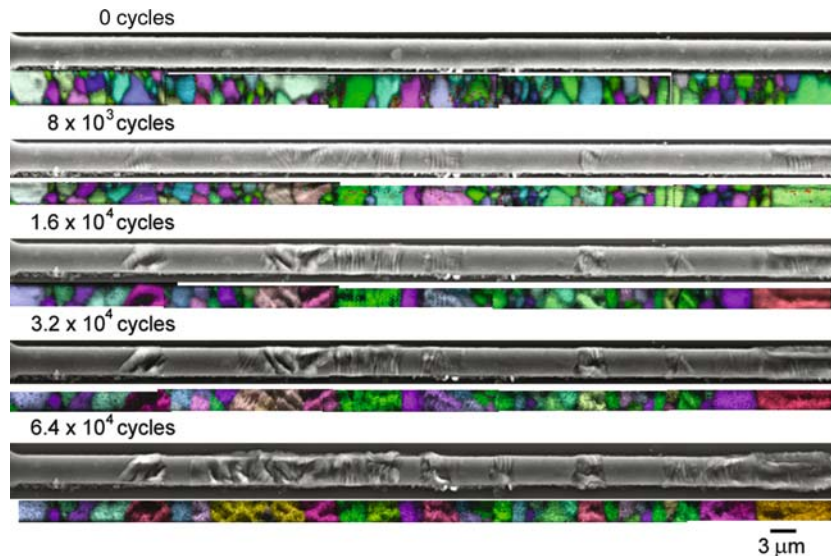


Fig. 1—SEM/orientation map pairs from the same region of the line, showing development of damage in the form of surface topography and grain growth/reorientation after 0, 40, 80, 160, and 320 s of accumulated cycling. Colors represent crystal directions lying parallel to line direction, with the legend given in Fig. 2. This $100\ \mu\text{m} \times 3\ \mu\text{m}$ region was used for all quantitative grain measurements.

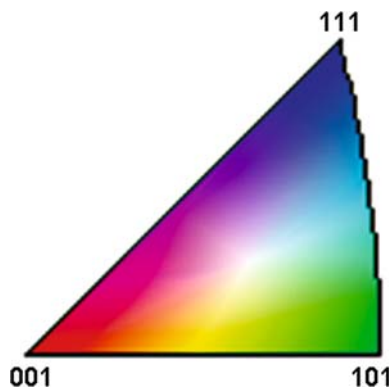


Fig. 2—Inverse pole figure legend for crystal directions lying parallel to the line direction, for orientation maps shown in Figs. 1 and 4.

Namely, damage is largely confined to individual grains, the spatial extent of such damage spreads with increased cycling, and the severity of topography increases with increased cycling. Note also that some grains exhibited orientation changes with increased cycling, as indicated by color changes.

A. Grain Size Measurements

Grain sizes were determined by use of the grain reconstruction method,^[14] wherein complete grains are identified by means of misorientation analysis, areas are calculated, and then equivalent circular diameters (ECDs) are calculated, inferring approximations of three-dimensional grain diameters. Table I shows the statistics associated with the evolution of grain size with cycling, over the targeted $100\ \mu\text{m} \times 3\ \mu\text{m}$ area. The maximum uncertainty in the ECD of a grain as determined by a single EBSD line scan across that grain is estimated to be twice the step size, or $0.4\ \mu\text{m}$.

However, this uncertainty decreases substantially when the grain reconstruction method is used, because the ECD depends on the grain area, which is far less sensitive to single pixel errors, especially for larger grains. Humphreys^[14] estimated an error in ECD of 10 pct when there are five EBSD steps across a grain and an error of 5 pct when there are eight EBSD steps across a grain. The mean grain diameters for the 0- and 320-second time-steps were 1.4 and $2.4\ \mu\text{m}$, and their distributions are shown in Figure 3. Our EBSD step size of $0.2\ \mu\text{m}$ suggests an error range of less than 10 pct, or less than approximately 0.14 to $0.24\ \mu\text{m}$ for average-sized grains throughout our tests. The accuracy will decrease accordingly for smaller grains in the population and increase for larger grains. However, for discussion of grain growth, only relative comparisons of changes in the populations are needed.

Distributions of grain diameters were lognormal (Anderson–Darling^[15] statistics ≤ 0.5 , p values ≥ 0.2) for the 0-, 10-, 20-, 40-, 80-, and 160-second time-steps. The data for the 320-second step did not fit a lognormal distribution as well as the other time-steps, exhibiting a p value of ≤ 0.1 . We attempted to fit the data to a Weibull distribution, as this distribution has in certain cases been shown to better describe grain size data than a lognormal distribution, for both as-patterned and annealed aluminum interconnects.^[16] However, the associated p value for that distribution was also less than or equal to 0.1, so we determined mean, median, and variance for the 320-second data by use of the relevant definitions for the lognormal distribution in order to maintain consistency.

Statistical analysis including all grains in the targeted region did not reveal significant global grain growth after 2000 thermal cycles (10 seconds of stressing). However, EBSD maps from some individual grains indicated that growth had started to occur locally, as shown by two examples in Figure 4. Grain A in the top pair of maps

Table I. Grain Size Statistics as a Function of Accumulated Cycles; Distributions through 3.2×10^4 Cycles are Lognormal; Neither Lognormal nor Weibull Distributions Fit Data Well for 6.4×10^4 Cycles; Diameters were Determined from EBSD Grain Area Measurements, Assuming Circular Grains

Total Cycles	Total Test Time (s)	Mean Diameter (Expected Value) (μm)	Median Diameter (μm)	Variance (μm)	Anderson–Darling Statistic for Lognormal Fit	p Value for Lognormal Fit
0	0	1.4	1.3	0.6	0.4	0.4
2×10^3	10	1.5	1.3	0.9	0.3	0.7
4×10^3	20	1.5	1.3	0.8	0.4	0.4
8×10^3	40	1.6	1.4	0.7	0.4	0.3
1.6×10^4	80	1.8	1.6	1.3	0.5	0.2
3.2×10^4	160	2.0	1.6	1.8	0.3	0.5
6.4×10^4	320	2.4*	2.0*	2.0*	1.2	< 0.1

*Values determined by use of definitions for lognormal distribution.

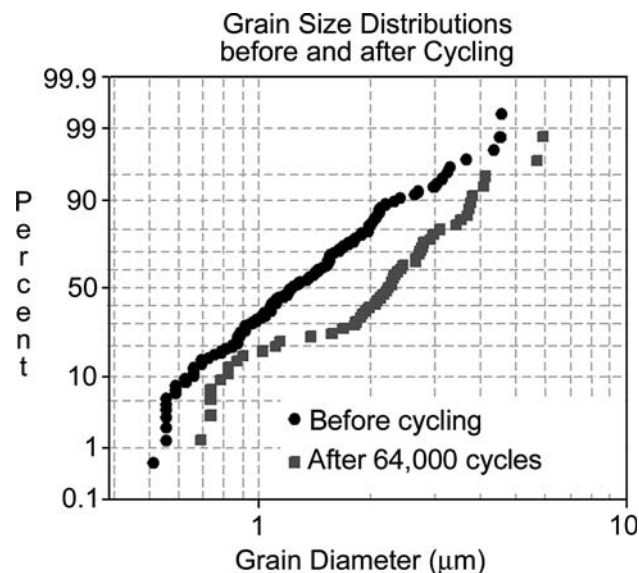


Fig. 3—Grain size distributions from the $100 \mu\text{m} \times 3 \mu\text{m}$ region of the line, before and after 6.4×10^4 thermal cycles at 200 Hz. The mean (expected value) grain diameter \pm measurement uncertainty increased from $1.4 \pm 0.4 \mu\text{m}$ to $2.4 \pm 0.4 \mu\text{m}$ after 320 s of cycling.

more than doubled its area during this time, with a corresponding increase in ECD of nearly 50 pct. Similarly, grain B in the bottom pair of maps showed an area increase of approximately 60 pct and corresponding increase in ECD of approximately 30 pct.

After 6.4×10^4 thermal cycles (320 seconds of stressing), both measures of central tendency indicated substantial increases in overall grain diameter as compared to the starting case; the lognormal mean increased by 71 pct and the lognormal median increased by 54 pct, as did the dispersion as measured by lognormal variance, which increased by > 300 pct. Such behavior in both central tendency and dispersion is to be expected during any competitive grain growth process, where some grains become larger by consuming their neighbors, which become smaller. Numerous examples of these changes can be seen in the sequence shown in Figure 1, where both growing and shrinking grains can be seen from one time-step to the next. Grains that have shown virtually no changes in size are also visible.

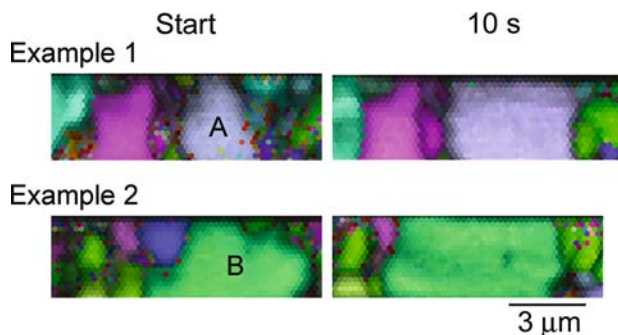


Fig. 4—EBSD maps showing two examples of grain growth that took place after 10 s of testing (2000 thermal cycles). Grain “A” shows an area increase of 114 pct, and equivalent diameter increase from $3.0 \mu\text{m}$ to $4.4 \mu\text{m}$. Grain “B” shows an area increase of 60 pct, and equivalent diameter increase from $4.0 \mu\text{m}$ to $5.2 \mu\text{m}$. Colors represent directions lying parallel to the line direction, with the legend given in Fig. 2.

B. Texture Measurements

Figure 5 shows inverse pole figures for surface normal directions in the as-deposited state (top) and after 1.39×10^5 cycles (bottom), demonstrating the evolution of texture with increased cycling. Prior to testing, the specimen exhibited a $\langle 111 \rangle$ fiber texture. The EBSD data taken selectively from regions that showed deformation revealed that such grains underwent rotation changes, with some even exceeding 40 deg after 1.39×10^5 thermal cycles, as indicated in the inverse pole figures. A detailed analysis of the plasticity mechanisms behind such rotations is underway and will be published separately. We conclude here that thermal cycling caused the initial fiber texture to significantly degrade.

C. Transmission Electron Microscopy

A TEM image from a region of the line that developed severe topography is shown in Figure 6, and an image from a region that showed negligible topography is shown in Figure 7. Both images were obtained from longitudinal cross sections prepared from the specimen after failure, *i.e.*, 1.39×10^5 thermal cycles. The bottom edge of each image represents the location of the film/substrate interface. The severity of the surface undulations in Figure 6 is evident. The local line thickness

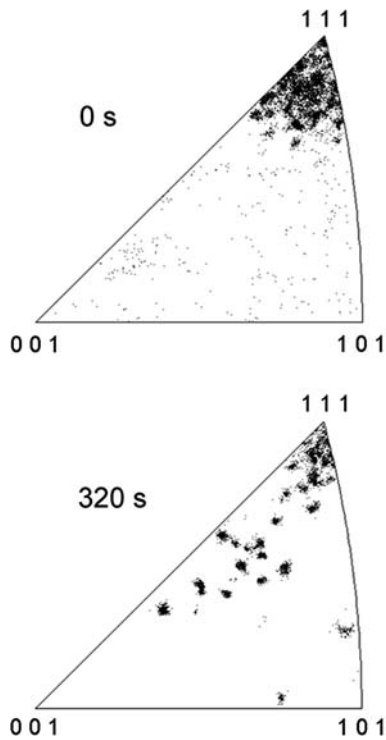


Fig. 5—Inverse pole figures showing surface normal orientations for grains prior to testing (top) and deformed grains after 1.39×10^5 thermal cycles (bottom), as determined by EBSD. Prior to cycling, the specimen showed a $\langle 111 \rangle$ fiber texture, typical of physical-vapor-deposited metals. After cycling, some grains rotated by more than 40 deg.

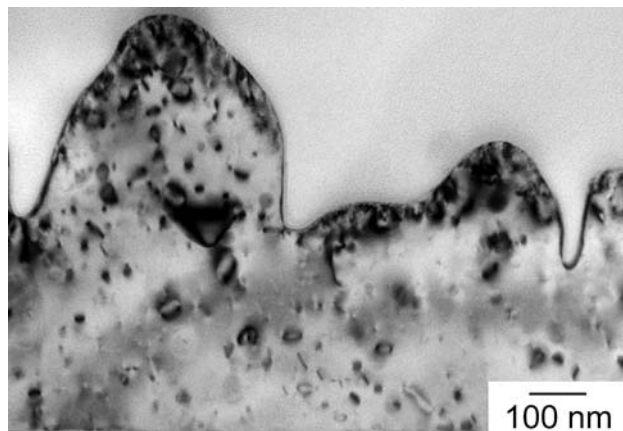


Fig. 6—Bright-field TEM image from a longitudinal cross section of a region of the line showing severe topography after 1.39×10^5 thermal cycles. Numerous prismatic dislocation loops are seen in this grain; however, there is negligible residual dislocation content in the form of segments. The image was taken approximately 6 months after testing, during which time loops grew from an initial average of approximately 4.5 nm to greater than 10 nm due to vacancy coalescence at room temperature. The bottom edge of the micrograph is coincident with the film/substrate interface.

varies substantially in regions such as this, with the large peak on the left of this figure corresponding to a local thickness of $0.73 \mu\text{m}$ and the sharp valley on the right of the figure corresponding to a local thickness of $0.28 \mu\text{m}$.

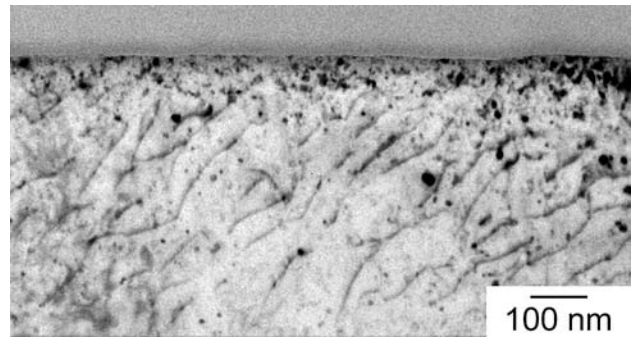


Fig. 7—Bright-field TEM image from a longitudinal cross section of a region of the line showing little topography after 1.39×10^5 thermal cycles. Numerous dislocation segments are visible in this grain. The bottom edge of the micrograph is coincident with the film/substrate interface.

Recall the initial line thickness was $0.5 \mu\text{m}$, determined by a stylus measurement. Note the presence of numerous vacancy prismatic dislocation loops, indicated by paired arc-shaped features. The image in Figure 6 was taken approximately 6 months after testing and shows loops of average diameter $> 10 \text{ nm}$. Similar images taken within weeks of testing revealed many smaller loops of diameter ~ 4 to 5 nm . The increase in average loop diameter during this time is consistent with observations of loop behavior in quenched aluminum, where gradual diffusion of lattice vacancies to larger loops at relatively low temperature caused the larger loops to grow at the expense of smaller loops.^[17] The image shown in Figure 7 was taken from the same specimen as that in Figure 6, yet shows a surface relatively free from undulations. The line thickness shows little variation from the initial $0.5\text{-}\mu\text{m}$ value. The image also shows the presence of numerous dislocation segments, as well as prismatic loops.

D. EBSD Image Quality and Grain Growth

We used EBSD pattern quality or “image quality” (IQ) in the particular system^[18] used here to evaluate the observed grain growth during cycling. The IQ parameter is a general means for quantifying the distinctness or clarity of the Kikuchi bands that appear within any given diffraction pattern. In order to better understand what the IQ parameter measures, we provide a brief summary of how the parameter is determined from an EBSD pattern, followed by how we used the term comparatively to evaluate grain growth.

For a given grain, each family of crystal planes gives rise to a Kikuchi band in the pattern, with the band intensity dependent on the backscattered electron yield associated with diffraction from that family of planes. The pattern is transformed into a Hough space representation, where each Kikuchi band becomes a peak in Hough space,^[19] with a unique axis-angle identifier. The intensity of each Hough peak scales with the average intensity of all pixels in the corresponding Kikuchi band in the diffraction pattern. The IQ parameter corresponds to the arithmetic average of the intensities, I_i , of all N

peaks present in the Hough space representation of a pattern, multiplied by a scaling factor, c :

$$IQ = \frac{\sum_i I_i \cdot c}{N} \quad [2]$$

In this work, the Hough space representation of each diffraction pattern typically contained $N < 12$ measurable peaks, and a constant scaling factor $c = 5$.

Several physical factors can cause a change in the average intensity of a Kikuchi band, and hence a change in the IQ parameter. In general, these factors affect the degree of crystal order contained within the information volume of the EBSD-specimen interaction space. We make the assumption here that the primary influence on IQ is the overall extent of residual stored plastic energy contained within each grain, hence the use of mean IQ within a grain. We discuss the validity of this assumption shortly. By residual stored plastic energy, we refer to defects such as dislocation segments, loops, or vacancies, all of which can be readily generated during cyclic deformation, and all of which have a localized elastic strain field about them. In terms of affecting the degree of local lattice order, a dislocation segment will have the greatest effect, followed by a small dislocation loop, and then a vacancy. We note that the loops observed in this work are vacancy prismatic loops, wherein lattice vacancies have coalesced to form the loop during rapid temperature changes.^[17]

Factors that can introduce errors in the use of grain-averaged IQ for evaluating stored plastic energy include the following: (1) if adjacent grains have significantly different thicknesses of aluminum oxide on their surfaces, then those covered by thicker oxide layers may show reduced IQ; (2) if a large proportion of a grain has severe elastic strain gradients within it, then it may show reduced IQ;^[20] (3) all (hkl) planes may not necessarily be affected uniformly by a given strain field or dislocation arrangement, which may cause some Hough peaks to have high intensity and others to have low intensity, for a given pattern, thereby causing possible inconsistency in the IQ; (4) stored plastic energy is often nonuniformly distributed even within a single grain, so a highly localized region of severe deformation can give rise to reduced IQ, while regions relatively free from deformation show an increased IQ; and (5) severe topography can degrade IQ by causing a shadowing effect on the detection of patterns; it can also degrade IQ if the individual asperities contain heavy dislocation content.

We find no reason to suspect that factor (1) or (2) plays a role, particularly in light of TEM observations made from similarly damaged specimens. We feel that factor (3) has not played a major role, because the TEM observations show that the differences in defect density from grain to grain (in the case where one grain has begun to consume its neighbor) are generally pronounced, likely overwhelming any effects of preferred defect orientation. If, however, adjacent grains contain a similar defect density, but significantly different orientations of those defects, then it is possible to see that orientation effect in the clarity of the Kikuchi bands, and therefore IQ parameter. We know that factor (4) does come into play,

upon viewing the localization effects of Figure 1. We initially suspected that factor (5) would play a large role; however, it did not. Sharp patterns were detected from regions of severe topography, despite shadowing effects, suggesting those regions did not contain significant dislocation content. A more accurate use of the IQ parameter for semiquantitatively measuring stored plastic energy would incorporate spatial correlations where regions nearer a grain boundary (but sufficiently removed from the strain field of the boundary itself) are weighted more heavily than those far from the boundary under consideration. However, we attempted the averaging method as a first-order approach.

We calculated the mean IQ value for each grain of a paired comparison where one grain began to consume its neighbor. As indicated above, we made 92 such comparisons for growing grains and 77 for grains that showed no relative growth. Figure 8 shows an example of a pairwise comparison between EBSD IQ factors. We consider the case of grain number 16 at the 80-second time increment. During cycling between 80 and 160 seconds, grain 16 grew toward its left, consuming grains 15 and 31, which are no longer present in the map representing the 160-second increment. Note that grain 16 at 80 seconds became grain 8 at 160 seconds. We determined the IQ values for all pixels contained in grains 16, 15, and 31 at the earlier time-step. Table II shows the IQ statistics. The mean value of the IQs for grain 16, measured at 80 seconds, is 89.1, while the mean values for grains 15 and 31 are 77.8 and 76.7, respectively. A one-tailed t -test comparing the IQ distributions for grains 16 and 15 under the hypothesis mean IQ (grain 16) < mean IQ (grain 15) resulted in a very low p value, suggesting that the mean IQ for grain 16 is not less than that for grain 15; we interpret this to functionally imply that the mean IQ for grain 16 is greater than that for grain 15. A similar analysis for the hypothesis mean IQ (grain 16) < mean IQ (grain 31) concluded that the mean IQ for grain 16 is functionally greater than that for grain 31.

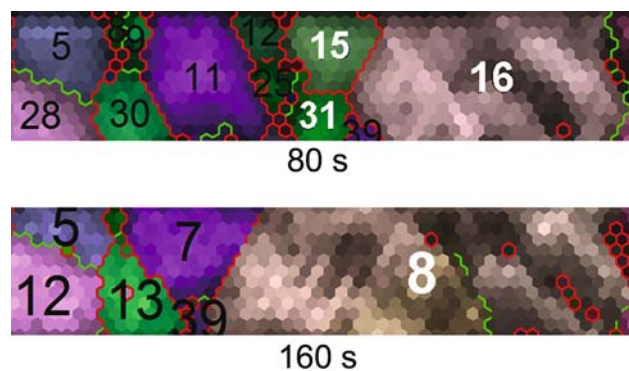


Fig. 8—Example of pairwise comparison of EBSD image quality parameters for growing grains. After the 80 s time increment, grain 16 grew, consuming grains 15 and 31 (among others). It became grain 8 at the 160-s time increment. The lines between grains indicate grain boundaries, with red corresponding to high-angle and green corresponding to low-angle boundaries. Boundaries surrounding single pixels are locations where the diffraction pattern could not be indexed.

Table II. EBSD Image Quality Statistics Corresponding to the Pairwise Comparisons Depicted in Figure 7; The p Values are Results for the One-Tail t -Tests that Consider the Cases IQ (Grain 16) < IQ (Grain 15) and IQ (Grain 16) < IQ (Grain 31)

Grain Number	Mean IQ	Standard Deviation of IQ	p Value
16	89.1	22.3	—
15	77.8	15.2	3.1×10^{-5}
31	76.7	11.4	2.8×10^{-5}

Table III(a). Pairwise EBSD Image Quality Statistics Corresponding to Comparisons of IQ Distributions for Neighboring Grains where Grain(1) Was Observed to Consume Grain(2), According to EBSD IQ Maps*

Test	Number of Cases	Proportion of Cases (Pct)	Confidence Level (Pct)
Total cases	92	100	—
Mean (1) > mean (2), no statistics	79	86	—
Mean (2) > mean (1), $p < 0.1$	69	75	90
Mean (2) > mean (1), $p < 0.05$	64	70	95
Mean (2) > mean (1), $p < 0.01$	60	65	99

*The term “mean (i)” represents the mean IQ value for grain (i), assuming normally distributed IQ values within that grain. The term p represents the p value for the hypothesis mean (2) > mean (1), incorporating a one-tailed t -test.

Similar pairwise comparisons were made for 90 other cases where one grain began to consume an adjacent grain, and the one-tailed t -test results shown in Table III (a). The results suggest that there are statistically significant differences between the mean IQ values for the cases considered, through the 99 pct confidence level. In most of those cases, the consumed grain statistically did not show a greater IQ value than that of the growing grain, as shown in the table; we interpret this to imply that the average IQ for growing grains was functionally greater than that of the consumed grains. We note here that no comparisons of IQ values were made between measurements made at different time-steps, as numerous microscope-related factors that vary with time make such comparisons invalid, *e.g.*, variations in probe current, working distance, EBSD calibration, *etc.*

Table III (b) includes control measurements for 77 cases, where no obvious grain growth took place between adjacent grains, according to the orientation maps. For the control cases, two-tailed t -tests were conducted under the hypothesis that the mean IQ value for one grain was less than that for an adjacent grain. Under such a hypothesis, the analysis suggested that in approximately half of the cases considered, the mean IQ value was not less than that for its neighbor at the 99 pct confidence level. In the absence of any biasing factors, 50 pct of the grains should be expected to have a higher IQ value than a given neighbor.

Table III(b). Pairwise EBSD Image Quality Statistics Corresponding to Comparisons of IQ Distributions for Neighboring Grains Where There was no Visual Indication that Grain (1) Consumed Grain (2) or *Vice Versa*, According to EBSD IQ Maps*

Test	Number of Cases	Proportion of Cases (Pct)	Confidence Level (Pct)
Total cases	77	100	—
Mean (1) > mean (2), no statistics	42	55	—
Mean (2) < mean (1), $p < 0.1$	47	61	90
Mean (2) < mean (1), $p < 0.05$	43	56	95
Mean (2) < mean (1), $p < 0.01$	38	49	99

*The term “mean (i)” represents the mean IQ value for grain (i), assuming normally distributed IQ values within that grain. The term p represents the p value for the hypothesis mean (2) < mean (1), incorporating a two-tailed t -test.

IV. DISCUSSION

Normal grain growth in thin physical-vapor-deposited metals is driven by minimization of interface or grain boundary energy, and exhibits a continuously monomodal grain size distribution during growth as well as negligible changes in crystallographic texture.^[21] A further characteristic of normal grain growth lies in the shapes of the moving boundaries. In the case of growth driven by minimization of grain boundary energies, boundaries move in the direction toward the concave side of the boundary, *i.e.*, in the direction of their center of curvature.

For the case of abnormal growth of such films, the grain size typically exhibits a distinct bimodal distribution at some point during growth, as thermal grooving selectively restricts grain boundary motion.^[22] The boundaries that remain mobile are those between grains with sufficiently different surface energies. In this case, only a small population of orientations remains amenable to growth. The crystallographic texture of abnormally grown grains typically has uniform fiber character.^[21]

Our measurements suggested that for several reasons, neither recrystallization nor normal nor abnormal grain growth occurred in our Al-1 at. pct Si lines during rapid thermal cycling. First, at no time, did we observe the formation of new grains during the course of tracking the evolution of microstructure throughout the experiments, evidenced by the quasi *in-situ* sequence shown in Figure 1. We note, however, that in isolated instances, subgrains appeared to develop during later stages of cycling, splitting a few of the very large grains. This is opposed to coalescing into larger grains, which is common during growth following recrystallization. Second, recrystallized grains are nominally strain free, having nucleated and grown to reduce stored strain energy. However, in the present tests, growing grains were associated with significant plasticity; we note that plasticity has taken place, resulting in the development of severe topography, but growing grains retained little

stored plastic energy. Finally, the conditions under which most of our results are reported (maximum temperature below 220 °C during less than 6 minutes of cycling, with an average temperature of approximately 120 °C) do not provide sufficient thermal energy to cause recrystallization. The temperature of 120 °C corresponds to a homologous temperature of 0.4 T_m , where T_m is the absolute melting temperature for aluminum (933 K). The values 0.4 to 0.5 T_m are approximately the temperature range one would expect for significant recrystallization in pure aluminum for a 1-hour hold time. However, after 320 seconds, we expect negligible changes to have occurred if conventional recrystallization was initiated. Furthermore, the 1 pct Si addition likely raises that temperature. We conclude therefore that no recrystallization has occurred.

The EBSD results indicated the presence of a monomodal distribution of grain diameter throughout the experiment. However, it is unlikely that the normal grain growth process took place, because we observed non-negligible plasticity in cycled lines. This was manifested through the severe surface topography and various forms of residual dislocation content. Normal grain growth is a process that is strictly driven by boundary energies. In the presence of plastic energy variations in the microstructure, the process is not dominant.^[23] Because the process depends on boundary energy, it is inherently curvature or surface-tension driven. We did not complete a comprehensive analysis of boundary orientation effects; however, there is evidence to suggest that boundaries of growing grains do not necessarily move toward the center of curvature. The trend is somewhat apparent in the sequence of Figures 1, 4, and 8. Therefore, it is unlikely that the observations correspond to the process of normal grain growth.

Some grains were observed to increase in diameter by a factor of greater than 6. This might suggest the operation of an abnormal growth process, where minimization of surface energy drives growth. The strongest argument against this process, however, is the observation of a monomodal distribution of grain sizes throughout the experiment. The next argument against abnormal growth is the observation of a significant weakening of the initial $\langle 111 \rangle$ fiber texture in grains that showed growth. These changes in orientation gradually developed during the experiment. No unusual orientations were observed at the onset. We will publish a detailed analysis of the re-orientation observations separately, which will emphasize such changes as a result of accumulating plasticity primarily through stage I dislocation slip. Finally, Kononenko and Matveev^[24] showed that abnormal growth can take place in high-purity aluminum after annealing at 400 °C for 1 hour. However, this is far more thermal energy than our conditions of 120 °C average temperature for less than 6 minutes. We conclude that the growth documented here is not consistent with abnormal grain growth.

We argue that the grain growth observed in our rapid thermal cycling experiments is consistent with strain-induced boundary migration. This is a process whereby the differences in stored plastic energy from grain to

grain drive boundary motion.^[25,26] We showed that it is reasonable to consider the average and median IQ values as tracking with total residual stored plastic strain energy contained in a grain. Analysis of IQ values on either side of moving boundaries revealed that there is a statistically significant trend: grains into which a boundary moved initially showed lower average and median IQ values than grains from which that boundary moved. The control measurements of IQ values for grains that showed no obvious growth indicated that in approximately half the cases, one grain had a higher IQ value than its neighbor from one time increment to the next. This is to be expected for situations where there is no factor having a significant effect on the IQ value.

That the grain into which a boundary moves has a lower average and median IQ value is also consistent with the TEM observations. Namely, the grain into which a boundary moved was typically the flatter of the two grains on either side of that boundary. Figures 6 and 7 show that the grains with flatter surface topography contained a higher density of dislocation segments than the grains that developed more severe surface topography. Such remaining dislocation content and the associated elastic distortion fields are sufficient to cause measurable degradation in EBSD IQ values. Figure 7 shows that in addition to a lack of residual dislocation segments in grains showing surface undulations, there is a considerable density of vacancy prismatic loops. These are typical remnants left behind in face-centered cubic metals that have undergone deformation by means of dislocation glide.^[27] The absence of significant residual dislocation segment content suggests that there was considerable glide taking place across the entire grain, with a significant Burgers vector component normal to the substrate, leading to accumulated surface displacements. The flat surface visible in Figure 6 suggests that whatever glide had taken place in that grain did not result in significant accumulated surface displacements. Instead, segments remained in the grain interior.

It is clear that considerable plastic deformation took place during rapid thermal cycling, and that the differences in stored plastic energy can account for the selectivity in grain growth. We discuss qualitatively possible reasons why some grains appeared to be more susceptible to retaining significant dislocation content than others. This is treated in terms of three factors: (1) dislocation sources, (2) resolved shear stress, and (3) local grain strength. In the plastic deformation of polycrystalline thin films, one must consider the interaction among these three factors as determining when a grain deforms and to what extent it deforms. Common operative dislocation sources in the absence of significant geometric defects (stress concentrations) include internal interfaces such as the film/substrate interface or grain boundaries. For the case of a biaxial tensile thermal stress in the plane of the film, grain boundaries are a likely cause for variation in efficiency of dislocation production from grain to grain. High-angle boundaries may be more likely to emit dislocations than a low-angle boundary, for example. The resolved shear stress is another factor that can vary strongly from grain to grain, for a given applied loading condition. This factor

plays a role even for strong fiber textures, as the in-plane orientation can vary considerably. Grains oriented such that high Schmid factor slip systems operate will yield first, in the case of equally operative dislocation sources and strengths. Finally, variations in strength are possible, due to localized variations in grain size, assuming an idealized Hall–Petch mechanism. Larger grains may be expected to yield first, in the case of equally operative dislocation sources and resolved shear stresses. We note that film thickness is not expected to play a role in grain to grain variability of strength, at least early in such a test, when grain surfaces remain relatively flat.

It is the combination of these factors that determines which grains yield first and to what extent they undergo plasticity. We can expect a range of degrees of deformation from grain to grain, based on how advanced the deformation becomes locally. The strain-induced boundary migration mechanism was correlated to relatively dislocation-free, distorted grains consuming grains that retained numerous dislocation segments and showed little distortion. Surface topography was accompanied by grain rotation, and both types of resultant plastic deformation can be accomplished largely through slip on a single family of slip planes, *i.e.*, akin to processes that take place during stage I strain hardening. The orientation effect can play a role in determining the extent of multiple slip taking place in a grain, thereby leading to dislocation interactions and barriers to further slip. This scenario is one example of how residual stored plastic energy could be left within a grain. While only suggestive at this point, this argument suggests some plausible reasons why deformation proceeded nonuniformly during cycling.

Strain-induced boundary migration may at least partially apply to the case of copper thermally cycled by alternating electric currents.^[11] In that work, (100) grains were observed to grow preferentially among grains that were predominantly $\langle 111 \rangle$ textured. For biaxial tension, (100) grains are expected to exhibit considerably lower in-plane strength compared to (111)-oriented grains, based on a comparison of orientation effects on strength of films.^[28] As such, they may yield first and undergo considerable stage I slip, leaving behind significant surface topography, as well as relatively strain-free material throughout the test. As (111) grains begin to deform, the (100) grains would have a driving force for growth. Without performing the measurements, however, we can only suggest this as speculation at this point.

V. SUMMARY AND CONCLUSIONS

We have shown the evolution of microstructure in nonpassivated Al-1 at. pct Si lines that have undergone rapid thermal cycling induced by alternating electric current. During 200 Hz cycling induced by alternating current with an rms density of 12.2 MA/cm², we observed rapid and significant growth of grains; mean grain diameters increased by greater than 70 pct after an accumulated cycling time of less than 6 minutes, as determined by automated EBSD. Growing grains

tended to develop plasticity in the form of topography and grain rotation, whereas those that showed little growth tended to show few changes to the original surface and orientation. The TEM observations showed that EBSD pattern quality could be correlated with the amount of residual dislocation content in individual grains of the deformed lines, with higher pattern quality corresponding to the presence of fewer dislocations. Through comparison of EBSD pattern quality, we found that growing grains showed lower residual dislocation content than the adjacent grains they consumed, at the 95 pct confidence level. This type of growth favors increasing the volume of material with little stored strain energy at the expense of material with higher strain energy (in the form of strain fields about dislocation cores). Growing grains were also observed to not necessarily grow in the direction of the center of curvature of their boundaries, as is usually seen for the case of normal grain growth. These factors suggest that the observed rapid growth of grains in thermally cycled aluminum alloy lines is consistent with strain-induced boundary migration, driven by the heterogeneous distribution of strain energy that results from local variations in individual grain strength, resolved shear stress, and efficiency of dislocation sources.

ACKNOWLEDGMENTS

We thank the NIST Office of Microelectronics Programs and the National Research Council Post-Doctoral Research Program for support. We thank D.S. Finch (AISthesis, LLC) for preparation of TEM specimens by FIB. This work is a contribution of the United States Department of Commerce and is not subject to copyright in the United States.

REFERENCES

1. F.R.N. Nabarro: *Theory of Crystal Dislocations*, Dover Publications, New York, NY, 1987, pp. 618–41.
2. A. Huang, Z. Suo, and Q. Ma: *J. Mech. Phys. Solids*, 2002, vol. 50, pp. 1079–98.
3. R.R. Keller, R. Mönig, C.A. Volkert, E. Arzt, R. Schwaiger, and O. Kraft: *Stress-Induced Phenomena in Metallizations: 6th Int. Workshop*, 2002, pp. 119–32.
4. P. Flinn: *J. Mater. Res.*, 1991, vol. 6, pp. 1498–1501.
5. D.S. Gardner and P.A. Flinn: *J. Appl. Phys.*, 1990, vol. 67, pp. 1831–44.
6. M. Thouless, J. Gupta, and J. Harper: *J. Mater. Res.*, 1993, vol. 8, pp. 1845–52.
7. A. Witvrouw, P. Flinn, and K. Maex: *MRS Symp. Proc.: Materials Reliability in Microelectronics VI*, Materials Research Society, Pittsburgh, PA, 1996, vol. 428, pp. 519–24.
8. R. Schwaiger and O. Kraft: *Acta Mater.*, 2003, vol. 51, pp. 195–206.
9. D.T. Read: *Int. J. Fatigue*, 1998, vol. 20, pp. 203–09.
10. R. Mönig, R.R. Keller, and C.A. Volkert: *Rev. Scientific Instrum.*, 2004, vol. 75, pp. 4997–5004.
11. Y.-B. Park, R. Mönig, and C.A. Volkert: *Thin Solid Films*, 2006, vol. 504, pp. 321–24.
12. R.R. Keller, R.H. Geiss, Y.W. Cheng, and D.T. Read: *MRS Symp. Proc.: Materials, Technology and Reliability of Advanced Interconnects*, Materials Research Society, Pittsburgh, PA, 2005, vol. 863, pp. 295–300.
13. ASTM F1259M-96R03 (2006) *Annual Book of ASTM Standards, ASTM*, Philadelphia, PA, vol. 10.04.

14. F. Humphreys: *J. Mater. Sci.*, 2001, vol. 36, pp. 3833–54.
15. NIST/SEMATECH e-Handbook of Statistical Methods, <http://www.itl.nist.gov/div898/handbook/>.
16. W. Fayad, V. Andleigh, C.V. Thompson, and H.J. Frost: *MRS Symp. Proc.: Materials Reliability in Microelectronics VIII*, 1998, vol. 516, pp. 159–64.
17. J. Silcox and M.J. Whelan: *Phil. Mag.*, 1960, vol. 5, pp. 1–28.
18. System manufactured by EDAX/TexSEM Labs. Commercial product names are provided in this work solely to clarify the nature of the measurements, specifically image quality, and do not imply endorsement by NIST or the United States Government.
19. N.C. Krieger Lassen: *Mater. Sci. Technol.*, 1996, vol. 12, pp. 837–43.
20. R.R. Keller, A. Roshko, R. Geiss, K. Bertness, and T.P. Quinn: *Microelectron. Eng.*, 2004, vol. 75, pp. 96–102.
21. H. Longworth and C.V. Thompson: *J. Appl. Phys.*, 1991, vol. 69, pp. 3929–40.
22. W.W. Mullins: *Acta Metall.*, 1958, vol. 6, pp. 414–27.
23. J.D. Verhoeven: *Fundamentals of Physical Metallurgy* Wiley, New York, NY, 1975, pp. 169–215.
24. O.V. Kononenko and V.N. Matveev: *MRS Symp. Proc.: Materials Reliability in Microelectronics VI*, 1996, vol. 428, pp. 231–36.
25. P.A. Beck and P.R. Sperry: *J. Appl. Phys.*, 1950, vol. 21, pp. 150–52.
26. C.C. Battaile, T.E. Buchheit, E.A. Holm, G.W. Wellman, and M.K. Neilsen: *MRS Symp. Proc.: Multiscale Modeling of Materials*, Materials Research Society, Pittsburgh, PA, 1999, vol. 538, pp. 269–73.
27. D. Kuhlmann-Wilsdorf and H.G.F. Wilsdorf: *Electron Microscopy and Strength of Crystals* Interscience, New York, NY, 1963, pp. 575–604.
28. J.E. Sanchez Jr. and E. Arzt: *Scripta Metall. Mater.*, 1992, vol. 27, pp. 285–90.